Supplementary Information for:

Biological Magnetometry: Torque on Superparamagnetic Beads in Magnetic Fields

Maarten M. van Oene[1], Laura E. Dickinson[1], Francesco Pedaci[1,2], Mariana Köber[1], David Dulin[1], Jan Lipfert[1,3,*], and Nynke H. Dekker[1,†]

[1]Department of Bionanoscience, Kavli Institute of Nanoscience, Delft University of Technology, Lorentzweg 1, 2628 CJ Delft, The Netherlands
[2]Department of Single-Molecule Biophysics, Centre de Biochimie Structurale, UMR 5048 CNRS, Montpellier, France
[3]Department of Physics and Center for NanoScience, Ludwig-Maximilian-University, Amalienstrasse 54, 80799 Munich, Germany

[*] Jan.Lipfert@lmu.de
[†] N.H.Dekker@tudelft.nl

Contents

S1 The Stoner-Wohlfarth model

Magnetic beads, such as those we employ, usually consist of magnetite (Fe_3O_4) or maghemite (γ-Fe_2O_3) nanoparticles ($\approx$ 8 nm) dispersed in a non-magnetic polymer matrix [1,2]. Here we numerically determine the torque on a single nanoparticle.

The torque on a nanoparticle is given by:

$$|\vec{\tau}| = \left|\vec{m} \times \vec{B}\right| = |\vec{m}|\left|\vec{B}\right| \sin\theta_2 \qquad \text{S1}$$

where $\vec{m}$ is the magnetic moment of the nanoparticle, $\vec{B}$ is the external magnetic field, and θ_2 is the angle between $\vec{m}$ and $\vec{B}$ (as indicated in Figure 1(a) of the main text). In the Stoner-Wohlfarth model [3], the magnetic moment $\vec{m}$ remains constant in magnitude, but its orientation depends on the orientation of the nanoparticle θ_{NP} (Figure 1(a)) and the external magnetic field $\vec{B}$. We numerically determined the orientation of the magnetic moment $\vec{m}$ and consequently the torque on a single nanoparticle based on the orientation of the anisotropy axis θ_{NP} and based on the magnetic field $\vec{B}$.

S1.1 The orientation of the magnetic moment

We assume the nanoparticle has a single magnetic moment and that the free energy of this single nanoparticle is given by **Equation 2** in the main text:

$$F = K \sin^2\theta_1 - |\vec{m}|\left|\vec{B}\right| \cos\theta_2 \qquad \text{S2}$$

where θ_1 and θ_2 are as indicated in Figure 1(a) of the main text, $K = \frac{1}{2}CV$ (where C is the anisotropy constant and V is the volume of the nanoparticle), and $|\vec{m}| = \left|\vec{M}\right|V$ (where $\vec{M}$ is the magnetization of the nanoparticle). We use $\sin^2 x = (1 - \cos 2x)/2$ to rewrite the equation for the free energy as:

$$\eta = 1 - \cos 2\theta_1 - h\cos\theta_2 \qquad \text{S3}$$

where $\eta = 2F/K$ and $h = 2|\vec{m}|\left|\vec{B}\right|/K$. Stoner and Wohlfarth already found that the magnetic moment will be in the same plane as the anisotropy axis and the magnetic field, hence $\theta_{NP} = \theta_1 + \theta_2$ [3].

To obtain the orientation θ_2 of the magnetic moment $\vec{m}$, we find the location of the energy minima for η. We use the first derivative of η:

$$\frac{\partial\eta}{\partial\theta_2} = 2\sin\big(2(\theta_{NP} - \theta_2)\big) + h\sin\theta_2 = 0 \qquad \text{S4}$$

An energy minimum is found, when the second derivative $\partial^2\eta/\partial\theta_2^2 > 0$. We find either one or two minima. At high absolute fields $\left|\vec{B}\right|$, only one energy minimum exists, and the angle θ_2 at which the minimum occurs, defines the orientation of the magnetic moment. If the absolute field $\left|\vec{B}\right|$ is decreased, a second energy minimum occurs, and the orientation of the magnetic moment depends on its previous orientation (and not on the depth of the energy wells), causing hysteresis in the system's response. Once we find the orientation θ_2 of the magnetic moment $\vec{m}$, we can calculate the torque using $|\vec{\tau}| = -|\vec{m}|\left|\vec{B}\right| \sin\theta_2$.

S1.2 High and low field approximations

For special cases, such as extreme values of h, there are analytical solutions for **Equation S4**, which allow us to predict and verify our numerical calculations in extreme regimes of h.

Generally, in the presence of an external field, there will be a competition between alignment of the magnetic dipole moment $\vec{m}$ with the external magnetic field $\vec{B}$ and alignment with the anisotropy axis. Depending on the values of K and $|\vec{m}||\vec{B}|$ in **Equation S2**, the dipole will align more with the anisotropy axis or more with the field.

S1.2.1 Torque on a single nanoparticle at low magnetic field

From Stoner and Wohlfarth [3], we know that $\theta_{NP} = \theta_1 + \theta_2$, so **Equation S4** can be written as:

$$2\sin(2\theta_1) = -h\sin\theta_2 \qquad \text{S5}$$

If $K \gg |\vec{m}||\vec{B}|$, so $h \approx 0$, then we can give an upper limit for θ_1, given that $|\sin x|_{\max} = 1$:

$$\theta_1 = \frac{1}{2}\operatorname{asin}\left(\frac{h}{2}\right) \qquad \text{S6}$$

So given $h \approx 0$, the upper limit for $\theta_1 \approx 0$. In this limit θ_2 can take all values, but θ_1 can only take a limited range of values close to zero, therefore the torque can be written, taking into account $\theta_2 \approx \theta_{NP}$, as:

$$|\vec{\tau}| = -|\vec{m}||\vec{B}|\sin\theta_{NP} \qquad \text{S7}$$

The magnetic torque is then set by the torque resulting from misalignment between the magnetic moment $\vec{m}$ and the external magnetic field $\vec{B}$. More intuitively, one can see that if $K \gg |\vec{m}||\vec{B}|$, the magnetic moment $\vec{m}$ will be strongly aligned with the anisotropy axis and the nanoparticle will essentially act as a permanent magnet.

S1.2.2 Torque on a single nanoparticle at high magnetic field

Starting with **Equation S5**, but now taking the limit in which $|\vec{m}||\vec{B}| \gg K$, so $h \gg 1$, we can give an upper limit for θ_2, given that $|\sin x|_{\max} = 1$:

$$\theta_2 = \operatorname{asin}\left(\frac{2}{h}\right) \qquad \text{S8}$$

So given $h \gg 1$, the upper limit for $\theta_2 \approx 0$. In this limit θ_1 can take all values, but θ_2 can only take a limited range of values close to zero, therefore the torque can be written, taking into account $\theta_1 \approx \theta_{NP}$, as:

$$|\vec{\tau}| = -K\sin 2\theta_{NP} \qquad \text{S9}$$

The maximum magnetic torque on a single nanoparticle will therefore become independent of the magnetic field $\vec{B}$. The maximum torque occurs at $\theta_{NP} = 45°$ and equals $|\vec{\tau}|_{max} = K$. The torque on the nanoparticle is then set by the torque resulting from misalignment between the magnetic moment $\vec{m}$ and the anisotropy axis. So the anisotropy axis, so to speak, "pulls" on the magnetic moment, but it cannot "pull" more strongly on the magnetic moment than $|\vec{\tau}|_{max} = K$.

S1.2.3 Torsional stiffness at high magnetic field near $\theta_{NP} = 0°$

The torsional stiffness κ_θ experienced by a single nanoparticle in high external fields can be derived from the expression for the torque at high fields by taking the derivative of **Equation S9**:

$$\kappa_\theta = -\frac{\partial \tau}{\partial \theta_{NP}} = K \cdot 2\cos 2\theta_{NP} \qquad \text{S10}$$

The torsional stiffness at high external fields near $\theta_{NP} = 0°$ can therefore simply be expressed as $|\kappa_\theta| = 2K$.

S1.3 Numerical simulations

S1.3.1 The torque as a function of h and θ_{NP}

In the simulations, we start with the nanoparticle aligned with the field, so $\theta_{NP} = 0$. Then we keep the field $\vec{B}$ constant, so h is constant, and rotate the nanoparticle over 2π. For each angle θ_{NP}, we determine the angle θ_2 of the magnetic moment $\vec{m}$. Once we obtained θ_2, we calculate the torque and normalize it by K:

$$|\vec{\tau}|/K = -\frac{|\vec{m}||\vec{B}|}{K}\sin\theta_2 = -\frac{h}{2}\sin\theta_2 \qquad \text{S11}$$

where $h = 2|\vec{m}|\left|\vec{B}\right|/K$. The results of the numerical simulations are shown in Figure S1. The graphs should be read from bottom to top, i.e. from $\theta_{NP} = 0$ to $\theta_{NP} = 2\pi$, because of hysteresis effects.

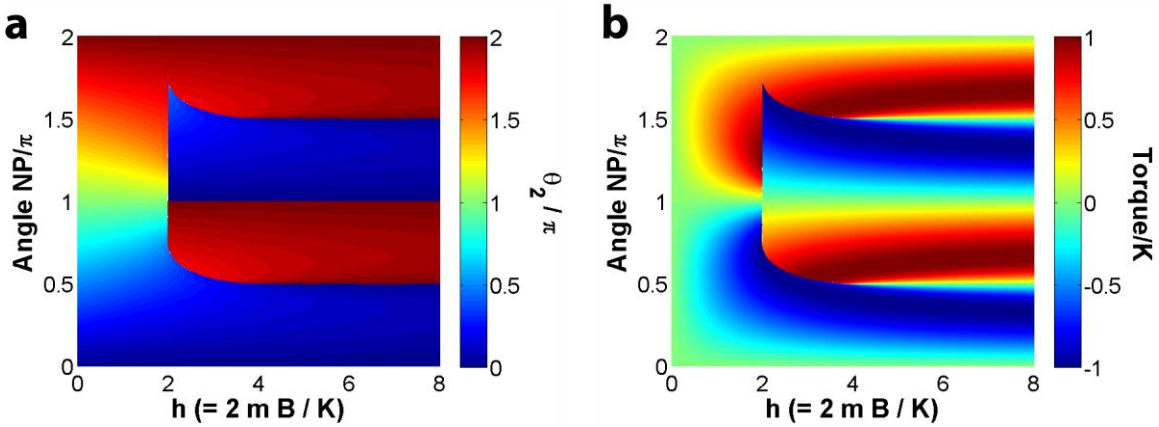

Figure S1 Heat maps for θ_2 and the torque on a nanoparticle. a) The angle θ_2 between the magnetic moment $\vec{m}$ and the external magnetic field $\vec{B}$ plotted as a function of the orientation of the nanoparticle θ_{NP} and the magnetic field $|\vec{B}|$, (or, equivalently, $h = 2|\vec{m}|\left|\vec{B}\right|/K$). b) The torque normalized by K plotted as a function of the orientation of the nanoparticle θ_{NP} and the magnetic field $|\vec{B}|$, (or, equivalently, $h = 2|\vec{m}|\left|\vec{B}\right|/K$).

In both plots we observe three regimes $h < 2$, $2 < h < 4$, and $h > 4$. In the first regime, where $h < 2$, we note that $|\vec{m}|\left|\vec{B}\right| < K$, so the anisotropy axis "pulls" strongly on the magnetic moment $\vec{m}$, and, for values of h closer to zero, the moment $\vec{m}$ will act more and more as a permanent moment. The angle θ_2 increases monotonically with the angle θ_{NP} of the nanoparticle (Figure S2.a). The torque plot is 2π-periodic and resembles the torque plot for a permanent magnetic moment m_0 (Figure S8) in this regime. In the second regime, where $2 < h < 4$, the orientation of the magnetic moment flips during rotation of the nanoparticle (Figure S2.b). This flipping also causes a sudden jump in the torque plot.

The torque plot is π-periodic. In the third regime $h > 4$, i.e. $|\vec{m}||\vec{B}| > 2K$, the magnetic moment $\vec{m}$ remains close to the magnetic field $\vec{B}$ and does not follow the rotation of the nanoparticle (Figure S2.c). The transitions of θ_2 at $\theta_{NP} = \frac{\pi}{2}, \pi,$ and $\frac{3\pi}{2}$, from $\theta_2 = 0$ (blue) to $\theta_2 = 2\pi$ (red) are not discontinuous, as the colour might suggest. The torque plot shows a π-periodic behaviour in this regime.

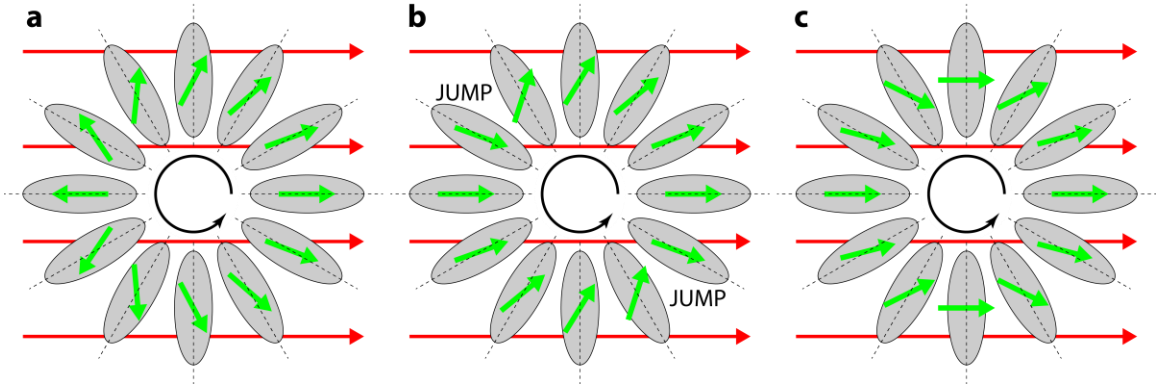

Figure S2 Rotation of a nanoparticle in a stationary magnetic field. a) For $h = 1.9$, the magnetic moment rotates along with the anisotropy axis. The grey ellipses are the nanoparticles at different orientations. Rotation of the nanoparticle starts at 0, i.e. alignment with the field. The red arrows indicate the stationary magnetic field $\vec{B}$. The green arrows are the magnetic moments of the nanoparticle at different orientations after rotation in the counter clockwise direction. b) For $h = 2.1$, the magnetic moment jumps to a different orientation between 4π/6 and 5π/6, and between 10π/6 and 11π/6. c) For $h = 4.1$, the magnetic moment remains closely aligned to the magnetic field during rotation of the nanoparticle.

S1.3.2 The torsional stiffness as a function of *h*

In Figure S3, we focus on the torque and the torsional stiffness. From the plot of the torque in Figure S1.b, we extract the torque as function of θ_{NP} for different values of h, (Figure S3.a). The derivatives of these curves near $\theta_{NP} = 0$ yield the stiffness for different values of h (Figure S3.b).

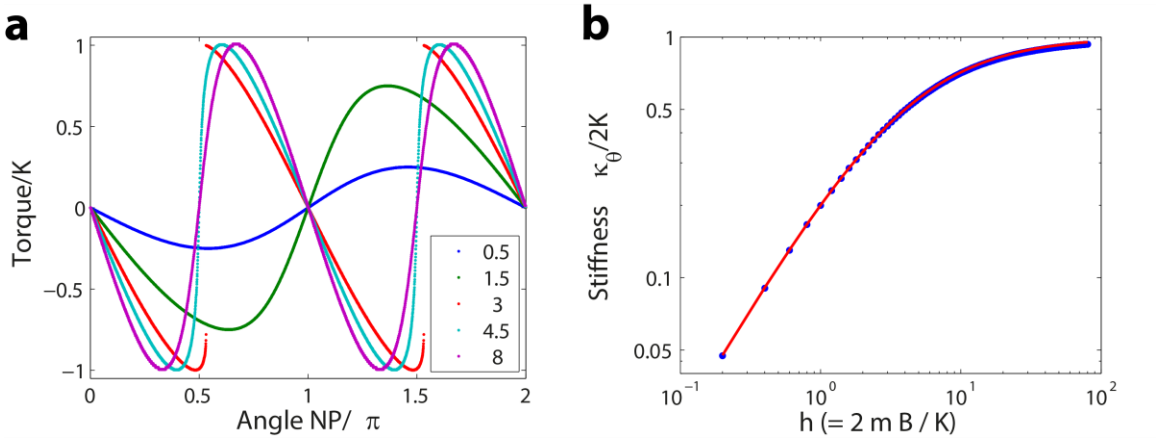

Figure S3 The torsional stiffness at different values of h. a) The torque dependence on θ_{NP} for different values of h indicated by the different colours (see legend). b) The stiffness dependence on h. The blue dots are the simulated data, and the red line is a co-plot of Equation S12.

Figure S3.a shows that for values of $h < 2$, the torque is 2π-periodic and closer to $h = 0$, the curves look more like $-\sin\theta_{NP}$, as expected (**S1.2.1**). Approaching $h = 2$, the minima of the curves shift toward $\theta_{NP} = 3\pi/4$ and the maxima towards $\theta_{NP} = 5\pi/4$. For values $2 < h < 4$, the curve becomes π-periodic and jumps in the torque occur

between π/2 and 3π/4. Beyond $h > 4$, the torque curve is continuous again and starts to resemble $-\sin 2\theta_{NP}$, as expected (**S1.2.2**).

In Figure S3.b, the simulated data agrees very well with the co-plot, which is derived from the small angle approximation of the stiffness, **Equation 3** in the main text:

$$\kappa_\theta = \frac{B\ C\ M\ N\ V}{C + M\ B} = \frac{B\ \frac{2K}{V}\frac{m}{V}\ N\ V}{\frac{2K}{V} + \frac{m}{V}B} = N\frac{2K\ mB}{2K + mB} = 2K\frac{2mB/K}{4 + 2mB/K} = 2K\frac{h}{4+h} \quad \text{S12}$$

where $K = \frac{1}{2}CV$, $m = MV$, $N = 1$, and $h = 2mB/K$. For low values of h, the stiffness increases linearly, as for a permanent magnetic moment. The stiffness $\kappa_\theta/2K$ approaches unity for larger values of h, as expected (**S1.2.3**).

S1.4 Mapping single nanoparticle behaviour to bead behaviour

We will simply assume that the anisotropy inside the magnetic bead arises from the anisotropy axes of the nanoparticles all pointing in the same direction. In addition, we will assume that all nanoparticles have the same $K = \frac{1}{2}CV$ and $m = MV$, and they do not interact with each other. The torque on the bead is then simply calculated by multiplying the torque on a single nanoparticle τ_{NP} by the number of nanoparticles N_{NP}, hence, $\tau_{magnets} = N_{NP}\tau_{NP}$.

S2 Numerical calculation of the torque on a single superparamagnetic nanoparticle

The torque on a superparamagnetic nanoparticle is again given by **Equation S1**. In contrast to the Stoner-Wohlfarth model, however, for a superparamagnetic nanoparticle, both the magnitude of the magnetic moment $|\langle\vec{m}\rangle|$ and the angle $\langle\theta_2\rangle$ change with the orientation of the nanoparticle θ_{NP} and the external magnetic field $\vec{B}$. Here we numerically calculate the magnitude of the magnetic moment $|\langle\vec{m}\rangle|$ and its orientation $\langle\theta_2\rangle$, based on the magnetic field $\vec{B}$ and the orientation of the anisotropy axis θ_{NP} (Figure 1(a) main text). The magnitude of the magnetic moment $|\langle\vec{m}\rangle|$ and the angle $\langle\theta_2\rangle$ are then used to calculate the torque on a single superparamagnetic nanoparticle.

S2.1 Mathematical procedure

We assume the nanoparticle has a single magnetic moment and that the free energy of this single nanoparticle is given by **Equation S2** [4]. In contrast to the Stoner-Wohlfarth model, we will use the magnitude of the expected magnetic moment here, which is dependent on the field $\vec{B}$ and the orientation θ_{NP}. The magnetic dipole can adopt all possible orientations $\vec{m} = \vec{m}(\theta, \phi)$, with θ ranging from 0 to π and ϕ ranging from 0 to 2π or, equivalently, from –π to π. The partition function for this nanoparticle is then given by:

$$Z = \int_0^{2\pi}\int_0^{\pi} \sin\theta \exp\left(-\frac{F}{k_B T}\right) d\theta\, d\phi. \quad \text{S13}$$

Consequently, the mean values for m_x, m_y and m_z are given by:

$$\langle m_x \rangle = \frac{1}{Z} \int_0^{2\pi} \int_0^{\pi} \sin\theta \exp\left(-\frac{F}{k_B T}\right) (|\vec{m}| \sin\theta \cos\phi) d\theta \, d\phi \quad \textbf{S14}$$

$$\langle m_y \rangle = \frac{1}{Z} \int_0^{2\pi} \int_0^{\pi} \sin\theta \exp\left(-\frac{F}{k_B T}\right) (|\vec{m}| \sin\theta \sin\phi) d\theta \, d\phi \quad \textbf{S15}$$

$$\langle m_z \rangle = \frac{1}{Z} \int_0^{2\pi} \int_0^{\pi} \sin\theta \exp\left(-\frac{F}{k_B T}\right) (|\vec{m}| \cos\theta) d\theta \, d\phi \quad \textbf{S16}$$

To compute these mean values, we perform numerical integrations over the surface of a sphere.

We define a coordinate system such that the magnetic field $\vec{B}$ is directed along the z-direction and the anisotropy axis of the magnetic nanoparticle lies in the yz-plane, i.e. $\phi_{NP} = \pi/2$. Increasing values of θ_{NP} then correspond to rotation of the magnetic nanoparticle in the yz-plane.

The numerical integration is performed for different values of $|\vec{B}|$ and θ_{NP}. For the numerical integration over the surface of a sphere we use Lebedev quadrature [5], which exploits a grid with a certain number of points, in our case 5810, where each point on the grid has a distinct weight. Summing over the whole grid, while taking into account the weights, we obtain an approximation to the surface integral over a sphere. For each point on the Lebedev grid, we convert its Cartesian coordinates to spherical coordinates; $\phi = \text{atan}(y/x)$, which returns values between –π and π; and $\theta = \text{acos}(z/r)$, which returns values between 0 and π. We use these spherical coordinates to calculate θ_1 and θ_2 for each point on the Lebedev grid. In this case we have $\theta = \theta_2$, since the field $\vec{B}$ is aligned with the z-axis. We then use the spherical law of cosines to calculate θ_1 using:

$$\theta_1 = \text{acos}(\cos\theta_{NP} \cos\theta + \sin\theta_{NP} \sin\theta \cos(\phi - \phi_{NP}))$$

Thus, if we set $\phi_{NP} = \pi/2$ and fix values for $|\vec{B}|$ and θ_{NP}, we can calculate θ_1, θ_2, and F for each point on the Lebedev grid and from this determine $\langle m_x \rangle$, $\langle m_y \rangle$ and $\langle m_z \rangle$ by numerical integration using Lebedev quadrature. Once we have found $\langle m_x \rangle$, $\langle m_y \rangle$ and $\langle m_z \rangle$, we convert those values to $|\langle \vec{m} \rangle| = \sqrt{\langle m_x \rangle^2 + \langle m_y \rangle^2 + \langle m_z \rangle^2}$, $\theta_2 = \text{acos}(\langle m_z \rangle / |\langle \vec{m} \rangle|)$ with values between 0 and π, and $\phi_\mu = \text{atan}\big(\langle m_y \rangle / \langle m_x \rangle\big)$ with values in the range from –π to π.

Using the obtained values for $|\langle \vec{m} \rangle|$, θ_2, and ϕ_μ, the magnitude of the torque can then be calculated according to **Equation S1.** In addition to the magnitude of the torque we would like to know the sign of the torque, since we know the axis along which the torque acts. If we define rotation about the x-axis from the positive y-axis towards the positive z-axis as an increase in θ_{NP}, then the one-dimensional torque along θ_{NP} is given by:

$$\vec{\tau} = \big(-\sin\phi_\mu\big) |\langle \vec{m} \rangle| |\vec{B}| \sin\theta_2 \quad \textbf{S17}$$

Alternatively, one can directly compute the following cross product to compute the torque once $\langle m_x \rangle$, $\langle m_y \rangle$ and $\langle m_z \rangle$ are known ($\langle m_x \rangle$ will be zero, because $\langle \vec{m} \rangle$ will be oriented between the field and the anisotropy axis in yz-plane. See Figure S4.c):

$$\vec{\tau} = \langle\vec{m}\rangle \times \vec{B} = \begin{vmatrix} \boldsymbol{i} & \boldsymbol{j} & \boldsymbol{k} \\ 0 & \langle m_y\rangle & \langle m_z\rangle \\ 0 & 0 & B_z \end{vmatrix} = \begin{vmatrix} \langle m_y\rangle & \langle m_z\rangle \\ 0 & B_z \end{vmatrix} \boldsymbol{i} = \langle m_y\rangle B_z \boldsymbol{i} \qquad \textbf{S18}$$

In both cases, in the single dimension of θ_{NP} (**Equation S17**) and in three dimensions (**Equation S18**), the torque is directed to align $\vec{m}$ with $\vec{B}$. The approach of calculating torque via $|\vec{m}|$, θ_2 and ϕ_μ is more cumbersome than using **Equation S18**, but provides more insight into what happens to the magnetic moment of the nanoparticle.

The values employed in the numerical calculations presented below are:
$k_B = 1.38 \cdot 10^{-23}\, J/K$, $T = 300K$, $|\vec{m}| = \frac{k_B T}{B_0}$ with $B_0 = 12\, mT$ [6] and $V = \frac{|\vec{m}|}{M_{sat}}$ with $M_{sat} = 43.3\, kA/m$ [6]. The number of nanoparticles $N_{NP} = 1$ and the values for $K = \frac{1}{2}CV$ are varied by varying C.

S2.2 High and low anisotropy constant approximations

For special cases involving particular values of θ_{NP} and/or extreme values of K, there are analytical solutions to our numerical calculations of the magnetic moment. For those cases, the analytical solutions provide a nice tool to predict and verify our numerical calculations.

S2.2.1 Magnetic moment as a function of magnetic field at $\theta_{NP} = 0°$ for $K \ll k_B T$

In the limit $K \ll k_B T$, the magnetic dipole is essentially free to rotate and orient in any direction. In the extreme case, when $K = 0$, **Equation S2** reduces to:

$$F = -|\vec{m}|\left|\vec{B}\right| \cos\theta_2 \qquad \textbf{S19}$$

In this case $\langle m_x\rangle = \langle m_y\rangle = 0$, and $\langle m_z\rangle$ can be solved analytically:

$$\langle m_z\rangle = |\vec{m}| L\left(|\vec{m}|\left|\vec{B}\right|\beta\right) = |\vec{m}|\left(\coth\left(\frac{|\vec{m}|\left|\vec{B}\right|}{k_B T}\right) - \frac{k_B T}{|\vec{m}|\left|\vec{B}\right|}\right) \qquad \textbf{S20}$$

where $L(x)$ is the Langevin function, $\beta = 1/k_B T$, and $\vec{B}$ points in the z-direction. In this case the magnetic dipole will act as a paramagnet.

S2.2.2 Magnetic moment as a function of magnetic field at $\theta_{NP} = 0°$ for $K \gg k_B T$

In the limit $K \gg k_B T$, the magnetic dipole will be aligned with the anisotropy axis and essentially only exists in one of two aligned states. With the magnetic field $\vec{B}$ pointing in the z-direction and $\theta_{NP} = 0°$, the situation will resemble a two-state paramagnet. In this case $\langle m_x\rangle = 0$, $\langle m_y\rangle = 0$, and $\langle m_z\rangle$ can be solved analytically, yielding:

$$\langle m_z\rangle = |\vec{m}| \tanh\left(\frac{|\vec{m}|\left|\vec{B}\right|}{k_B T}\right) \qquad \textbf{S21}$$

Note that if $K \gg k_B T$, the dipole might not be able to flip between the two aligned states on the timescale of the experiment due to a long Néel relaxation time [7].

S2.3 Numerical calculations

S2.3.1 $|m|$, θ_2, ϕ_μ and torque as a function of magnetic field and orientation of the nanoparticle θ_{NP}

The numerical calculations are performed for three values of C: one value of C similar to the value found by fitting to the experimental data, and one value lower and one value higher than the fitted C. The value similar to the fitted value is $C = 3 \cdot 10^3\ J/m^3$, the value higher is $C = 3 \cdot 10^4\ J/m^3$, and the lower value is $C = 0\ J/m^3$. This low value serves as an internal check on the simulations.

Figure S4(i) shows the calculations for $C = 0\ J/m^3$, in which case the magnetic dipole should act as a pure paramagnet. This paramagnetic case is an internal check on our calculations. In the first plot (Figure S4.a(i)), $|\vec{m}|$ only depends on the magnetic field $|\vec{B}|$, but not on the angle of the nanoparticle θ_{NP}. In the second plot (Figure S4.b(i)), θ_2 is 0 for positive fields and π for negative fields, which means the dipole moment is always aligned with the external field. In the third plot (Figure S4.c(i)), ϕ_μ takes on various values, probably because the dipole moment is aligned with the z-axis and ϕ_μ is not really defined in that case. In the fourth plot (Figure S4.d(i)), the torque is zero everywhere, since the dipole moment is always aligned with the external field. These results all agree with the expectations for a paramagnet, indicating a correct implementation of the method used for further calculations.

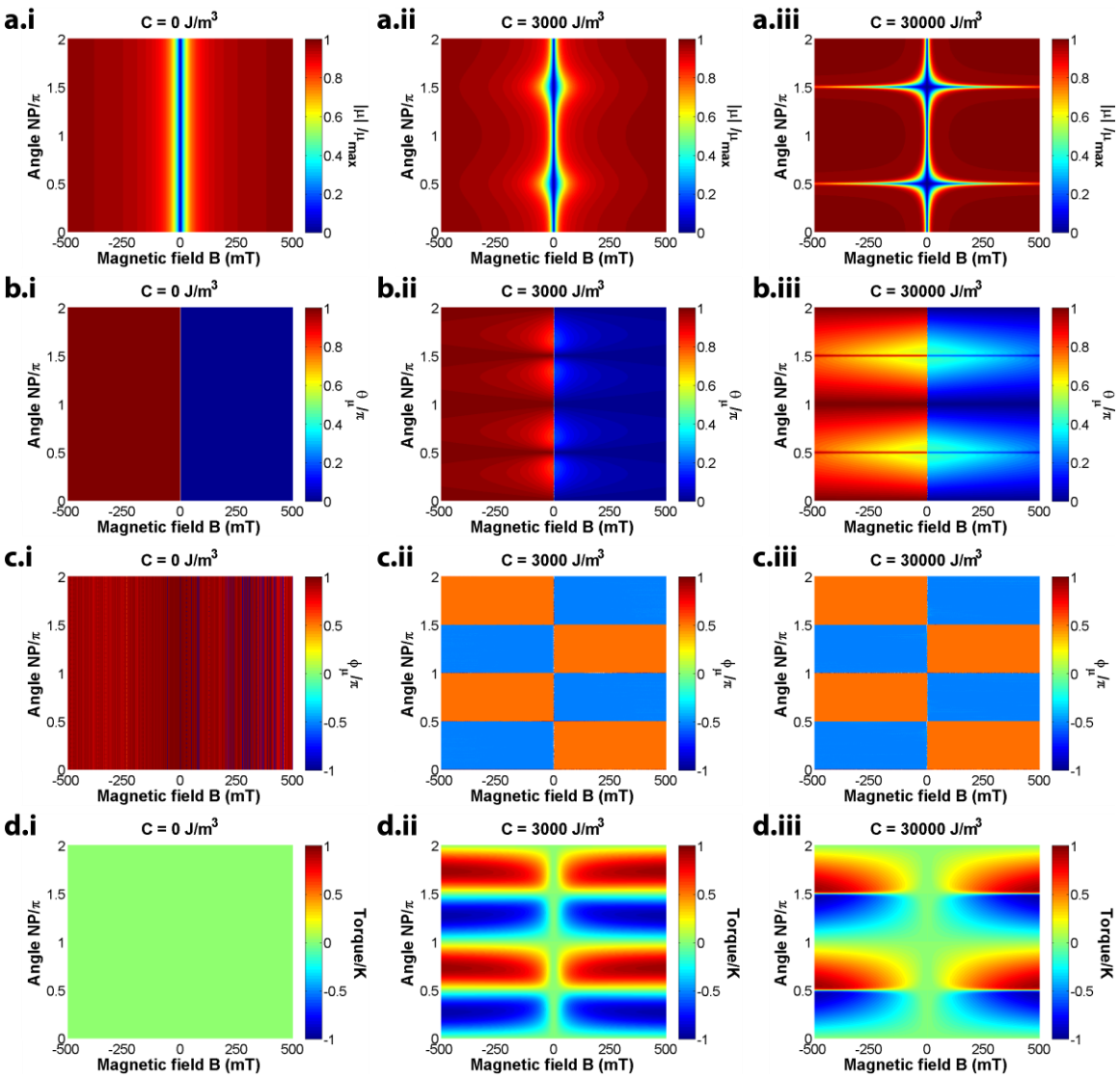

Figure S4 Heat maps for the magnetic moment and torque on a superparamagnetic nanoparticle. The columns of this figure are calculations for different values of C, the values are i) $C = 0\ J/m^3$, ii) $C = 3 \cdot 10^3\ J/m^3$ and iii) $C = 3 \cdot 10^4\ J/m^3$. The rows of this figure display a) The magnitude of the magnetic moment $|\vec{m}|$ normalized by its maximum value, b) θ_2 divided by π, c) ϕ_μ divided by π and d) the torque normalized by K. In all plots the magnetic field runs from $B = -500\ mT$ to $B = 500\ mT$ and the angle of the nanoparticle θ_{NP} runs from 0 to 2π.

In Figure S4(ii) and Figure S4(iii), $C = 3 \cdot 10^3\ J/m^3$ and $C = 3 \cdot 10^4\ J/m^3$, respectively. In the first row, the value of $|\vec{m}|$ decreases, going from 0, π or 2π towards π/2 or 3π/2. This decrease is stronger for higher values of C. At higher fields, the value of $|\vec{m}|$ still reaches its maximum value m_{max}. If $K = \frac{1}{2}CV$ is large compared to $|\vec{m}||\vec{B}|$, the dipole prefers to align with the anisotropy axis. The external field $\vec{B}$ then determines which of the aligned states is preferred. Closer to $\theta_{NP} = \frac{\pi}{2}$, the energetic difference between the two states decreases and therefore the preference for either one of the states is reduced. As a result, the populations in the two states cancel each other, resulting in a decrease of the net $|\vec{m}|$ around π/2 and 3π/2.

In Figure S4.b, θ_2 is still close to 0 for positive fields and close to π for negative fields, which means the dipole moment tends to align with the external field. In reality the dipole is only well aligned with the field at $\theta_{NP} = 0$, π/2, π, 3π/2 or 2π. At intermediate angles, the anisotropy energy prevents the dipole from perfect alignment with the external field. As C increases, the energetic penalty for misalignment between dipole and anisotropy axis is larger. The anisotropy axis "pulls" more strongly on the dipole, which results in a larger angle θ_2 between dipole and external field for larger C.

In Figure S4.c, ϕ_μ is either –π/2 or π/2, which in both cases means the net dipole moment lies in the yz-plane. This is expected, since we set the anisotropy axis of the nanoparticle to rotate in the yz-plane, i.e. $\phi_{NP} = \pi/2$.

In Figure S4.d, the torque is in both cases ($C = 3 \cdot 10^3\ J/m^3$ and $C = 3 \cdot 10^4\ J/m^3$) directed to orient the nanoparticle at 0, π or 2π, i.e. to align the anisotropy axis with the external field. At π/2 and 3π/2, the torque is zero, but, as these are unstable trapping positions, small deviations from these angles will force the nanoparticle to rotate away.

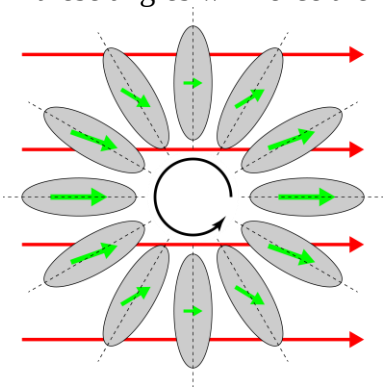

Figure S5 Rotation of a nanoparticle in a stationary magnetic field. The grey ellipses are the nanoparticles at different orientations. The red arrows indicate the stationary magnetic field $\vec{B}$. The green arrows are the magnetic moments of the nanoparticle at different orientations. The magnetic dipole moment changes both orientation and magnitude during rotation.

S2.3.2 The net magnetic moment as a function of the external magnetic field at $\theta_{NP} = 0°$

The plot for $|\vec{m}|$ in Figure S4.a can be used to obtain the magnetization curve. The magnetization $|\vec{M}| = |\vec{M}|(|\vec{B}|)$ is an important parameter in **Equation 3** of the main text, which is used to fit the experimental data for the torsional stiffness. For the fitting procedure, we would prefer an analytical expression for $|\vec{M}|(|\vec{B}|)$. The curve shown in Figure S6 is the lowest row ($\theta_{NP} = 0°$) of the plot of $|\vec{m}|$ in Figure S4.a, with the slight difference that $|\vec{m}|$ can attain a negative value in Figure S6.

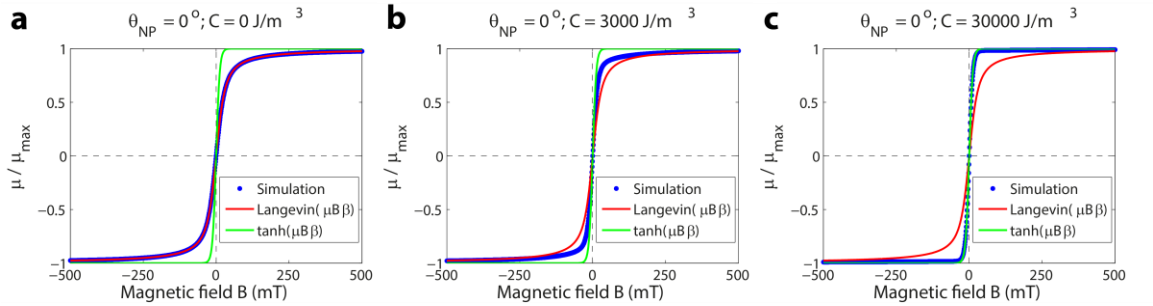

Figure S6 Magnetization curves of superparamagnetic nanoparticles with different values of the anisotropy constant C. In the legends of the plots $\beta = 1/k_B T$. a) In the first plot, the calculated m agrees very well with the Langevin function derived for a paramagnet. This result provides an additional confirmation that our numerical calculations are correct. b) In the second plot $C = 3 \cdot 10^3\ J/m^3$, the calculated value of $|\vec{m}|$ lies in between the prediction for a classical paramagnet, the Langevin function, and the prediction for a two-state paramagnet, the hyperbolic tangent. This result shows how C effects the magnetic moment dependence on the field. c) In the third plot $C = 3 \cdot 10^4\ J/m^3$ and the calculated $|\vec{m}|$ agrees well with the hyperbolic tangent derived for a two-state paramagnet. This result agrees with our expectations for $K \gg k_B T$ and confirms the correctness of our computational approach. Again, we should note that the calculations assume a situation in which the dipole can thermally explore all orientations, while in reality the dipole might not be able to flip between the two states on the time scale of our measurements.

S2.3.3 The torque and torsional stiffness dependence on the magnetic field and nanoparticle orientation θ_{NP}

In Figure S7, we focus on the magnetic torque $\vec{\tau}$ and the torsional stiffness κ_θ, and their dependence on the nanoparticle orientation θ_{NP} and on the magnetic field $\vec{B}$. The results in Figure S7(i) are based on calculations with $C = 3 \cdot 10^3\ J/m^3$, and in Figure S7(ii) the results are based on calculations with $C = 3 \cdot 10^4\ J/m^3$.

In Figure S7.a, we plot the torque as a function of the nanoparticle orientation θ_{NP} for different magnetic field strengths. Here each curve in Figure S7.a is a column of the plot for the torque (Figure S4.d), corresponding to a certain magnetic field strength $|\vec{B}|$. The torque is normalized by its maximum value for that particular field strength. The graphs resemble $\sin(2\theta)$-functions, but have different degrees of skew depending on the strength of the magnetic field. The angular position at which the maximum torque occurs, shifts with field strength. For small absolute fields, the angle of maximum torque is 45°. For such small absolute values of the field ($|\vec{B}| < B_0$), the magnetization is linear in the field $\vec{M} = \chi\vec{B}$, where χ is a tensor. The torque is then proportional to $\chi\vec{B} \times \vec{B}$, which is again proportional to $\sin(2\theta)$, where θ is the angle between field $\vec{B}$ and anisotropy axis. This proportionality, $\tau \propto \sin(2\theta_{NP})$, explains the maximum torque at 45° for small fields. When the magnetic field strength is increased, this angle increases towards, but does not reach, 90°. Increasing the external magnetic field $\vec{B}$ further until $|\vec{B}||\vec{M}| \gg C$, the magnetic torque becomes "stronger" than the torque by the anisotropy axis. As expected from **S1.2.2**, at such high fields the maximum torque occurs again at 45°.

In Figure S7.b, we plot the torsional stiffness κ_θ as a function of the magnetic field $|\vec{B}|$ on a log-log scale. This plot is again deduced from the plot for the torque (Figure S4.d). The stiffness is computed by taking the derivative along the columns, and we are interested in its value near $\theta_{NP} = 0$. More specifically, to obtain the stiffness near $\theta_{NP} = 0$, the torque in the bottom row ($\theta_{NP} = 0$) is subtracted from the torque in the row above and divided by $d\theta$, i.e. we take the numerical derivative at $\theta_{NP} = 0$. The value of

$\kappa_\theta/2K$ approaches unity for increasing magnetic fields. This result confirms our expectation that the maximum torsional stiffness should occur at $|\kappa_\theta| = 2K$. For larger values of C, higher magnetic fields are measured to reach the maximum torsional stiffness. The torsional stiffness is fitted to an expression derived in the small angle approximation [4]:

$$\kappa_\theta = N\,V\,\frac{C\,|\vec{B}||\vec{M}|}{C + |\vec{B}||\vec{M}|} \qquad \text{S22}$$

where $N = N_{NP} = 1$, and C and NV are fitting parameters. For $|\vec{M}|$ we used either **Equation S23** or **S24**, fits for both are shown. We observe that the hyperbolic tangent $|\vec{M}|$ fit to the torsional stiffness for $C = 3 \cdot 10^4\ J/m^3$ provides the best match. This result was expected, since the data for $C = 3 \cdot 10^4\ J/m^3$ also provided the best match to the hyperbolic tangent $|\vec{M}|$ in Figure S6. Deviations of the fits in Figure S7.b likely result from deviations between the numerical calculations and analytical cases in Figure S6.

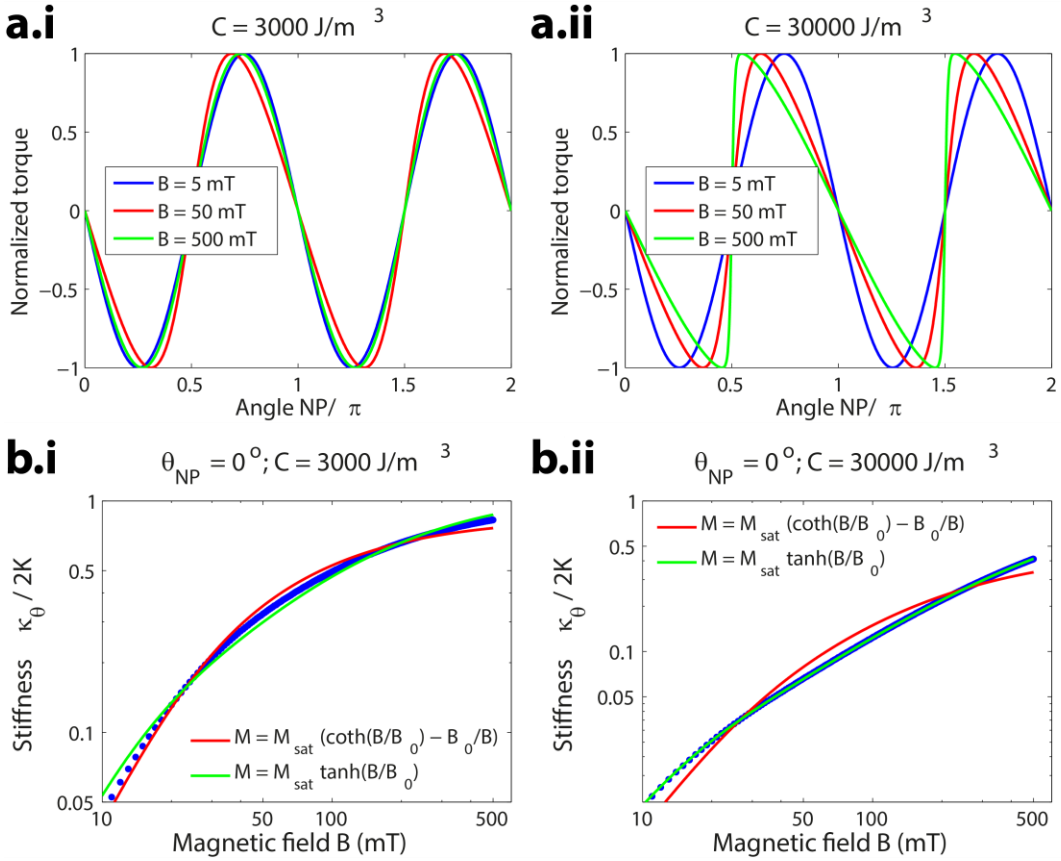

Figure S7 The columns of this figure are calculations for different values of C, i) $C = 3 \cdot 10^3\ J/m^3$ and ii) $C = 3 \cdot 10^4\ J/m^3$. From top to bottom the rows show: a) normalized torque versus angle of the nanoparticle θ_{NP}; b) the stiffness as a function of the magnetic field.

Different expressions of $|\vec{M}|$ in **Equation S22** give slightly different outcomes for the torsional stiffness κ_θ. We can use a classical paramagnetic interpretation similar to **Equation S20**:

$$\left|\vec{M}\right| = M_{sat}\left(\coth\left(\frac{\left|\vec{B}\right|}{B_0}\right) - \frac{B_0}{\left|\vec{B}\right|}\right) \quad \text{S23}$$

with M_{sat} the saturation magnetization and $B_0 = k_B T/|\vec{m}|$. For large magnetic fields $\left|\vec{B}\right|$, the magnetization saturates at M_{sat}. For small magnetic fields, the magnetization goes as $\left|\vec{M}\right| = M_{sat}\left|\vec{B}\right|/3B_0$. Therefore, $\kappa_\theta \propto \left|\vec{B}\right|^2$ at low fields. We can also use a two-state paramagnet interpretation similar to **Equation S21**:

$$\left|\vec{M}\right| = M_{sat}\tanh\left(\frac{\left|\vec{B}\right|}{B_0}\right). \quad \text{S24}$$

Again, for large fields, the magnetization saturates at M_{sat}. For small fields, the magnetization goes as $\left|\vec{M}\right| = M_{sat}\left|\vec{B}\right|/B_0$ and again $\kappa_\theta \propto \left|\vec{B}\right|^2$. In contrast, in the Stoner-Wohlfarth model, the magnetization is constant:

$$\left|\vec{M}\right| = M_{sat}. \quad \text{S25}$$

At small magnetic fields, the torsional stiffness $\kappa_\theta \propto \left|\vec{B}\right|$ (see Figure S3.b). For all interpretations of the magnetization $\left|\vec{M}\right|$, the stiffness κ_θ saturates at high magnetic fields, because then $\kappa_\theta \approx C\,N\,V$.

S2.4 Mapping single nanoparticle behaviour to bead behaviour

When this model was proposed for superparamagnetic beads [4], the authors posed the assumption that all nanoparticles inside the magnetic bead have their anisotropy axes pointing in the same direction, have the same $K = \frac{1}{2}CV$ and $m = MV$, and do not interact with each other. The torque on the bead is then simply calculated by multiplying the torque on a single nanoparticle τ_{NP} by the number of nanoparticles N_{NP}, hence, $\tau_{magnets} = N_{NP}\tau_{NP}$.

S3 Calculation of the torque on a permanent magnetic moment

As a reference point for comparison to Figure S1 and Figure S3, here we provide the equivalent figures for a permanent magnetic moment.

S3.1 The torque as a function of B and θ_{NP}

In the model with the permanent magnetic moment m_0, the angle $\theta_1 = 0$ and $\theta_2 = \theta_{NP}$. The torque is given by **Equation S7**:

$$\tau = -m_0 B\sin\theta_2 = -m_0 B\sin\theta_{NP} \quad \text{S26}$$

so the torque will be 2π-periodic.

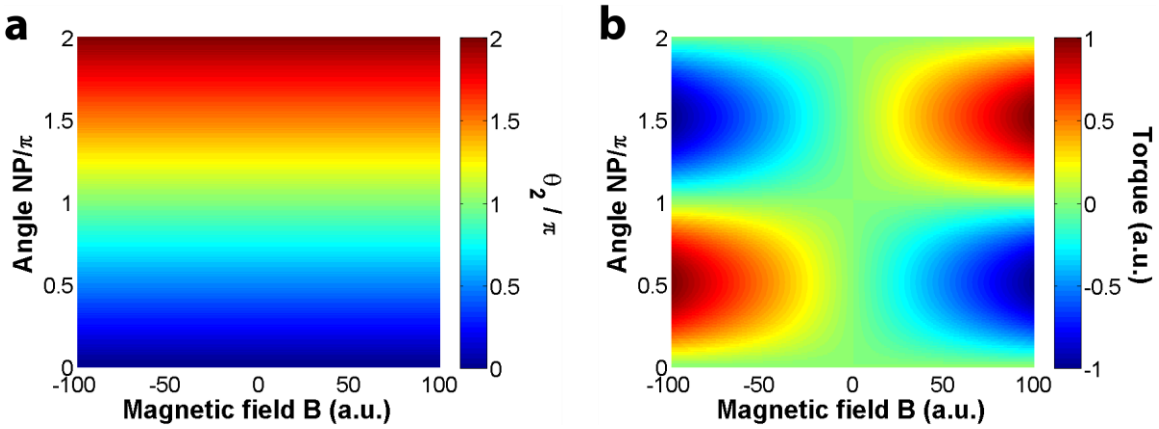

Figure S8 Heat maps for θ_2 and the torque on a permanent magnetic moment. a) The angle θ_2 between the magnetic moment $\vec{m}$ and the external magnetic field $\vec{B}$ as a function of the orientation of the nanoparticle θ_{NP} and the magnetic field $|\vec{B}|$. b) The torque as a function of the orientation of the nanoparticle θ_{NP} and the magnetic field $|\vec{B}|$.

S3.2 The torsional stiffness as a function of *B*

In Figure S9, we focus on the torque and the stiffness. From the plot of the torque in Figure S8.b, we extract the torque as function of θ_{NP} for different values of $|\vec{B}|$ (Figure S9.a). The derivatives of these curves near $\theta_{NP} = 0$, give the stiffness for different values of $|\vec{B}|$, as plotted in Figure S9.b. The torsional stiffness should equal $\kappa_\theta = m_0 B$ and therefore be linear in the field $|\vec{B}|$.

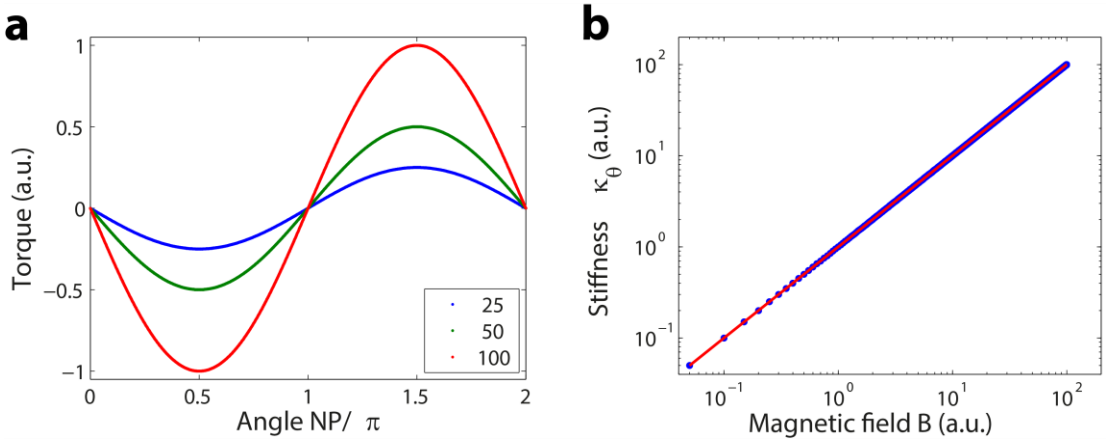

Figure S9 The torsional stiffness at different values of the magnetic field $|\vec{B}|$. a) The torque dependence on θ_{NP} for different values of $|\vec{B}|$ indicated by the different colours and the legend. b) The stiffness dependence on $|\vec{B}|$. The blue dots are the data obtained via Figure S9.a and the red line is a co-plot of $\kappa_\theta = m_0 B$ with $m_0 = 1$.

S3.3 Mapping single nanoparticle behaviour to whole bead behaviour

When this model was proposed for superparamagnetic beads [8], the authors assumed a single permanent moment for the whole bead, which is equivalent to simply multiplying the moment of a single nanoparticle by the "effective" number of nanoparticles N_{NP} contributing to the torque.

S4 Simulation of the torque on a nanoparticle with a rectangular hysteresis curve

As a reference point for comparison to Figure S1 and Figure S3, here we provide the equivalent figures for a nanoparticle with a rectangular hysteresis curve.

S4.1 The torque as a function of B and θ_{NP}

In this model, the nanoparticle has a rectangular hysteresis curve (Figure S10) irrespective of its angular orientation. The magnetic dipole moment only strictly exists in the two states aligned with the anisotropy axis. Flipping between the two states requires a component of the external magnetic field along the anisotropy axis which is larger than the coercive field $\left|\vec{B}_{\text{coercive}}\right|$. Below the coercive field, the bead acts as though it has a permanent magnetic moment.

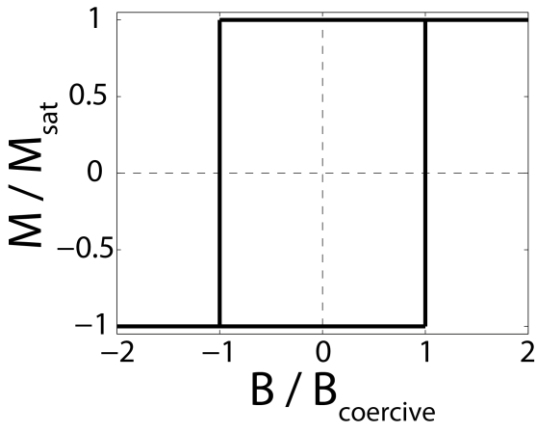

Figure S10 Rectangular hysteresis curve. The magnetization along the anisotropy axis is plotted as a function of the magnetic field along the anisotropy axis. The magnetization is normalized by the saturation magnetization M_{sat} and the magnetic field is normalized by the coercive field B_{coercive}. Flipping of the magnetization between the two states aligned with the anisotropy axis occurs at $|B/B_{\text{coercive}}| = 1$.

In the simulations, we start with the nanoparticle aligned with the field, so $\theta_{NP} = 0$. Then we keep the field $\vec{B}$ constant, so B/B_{coercive} is constant, and rotate the nanoparticle over 2π. At each angle θ_{NP}, we determine the angle θ_2 of the magnetic moment $\vec{m}$. Once we obtained θ_2, we calculate the torque. The results of the numerical simulations are shown in Figure S11. The graphs should be read from bottom to top, i.e. from $\theta_{NP} = 0$ to $\theta_{NP} = 2\pi$, because of hysteresis effects.

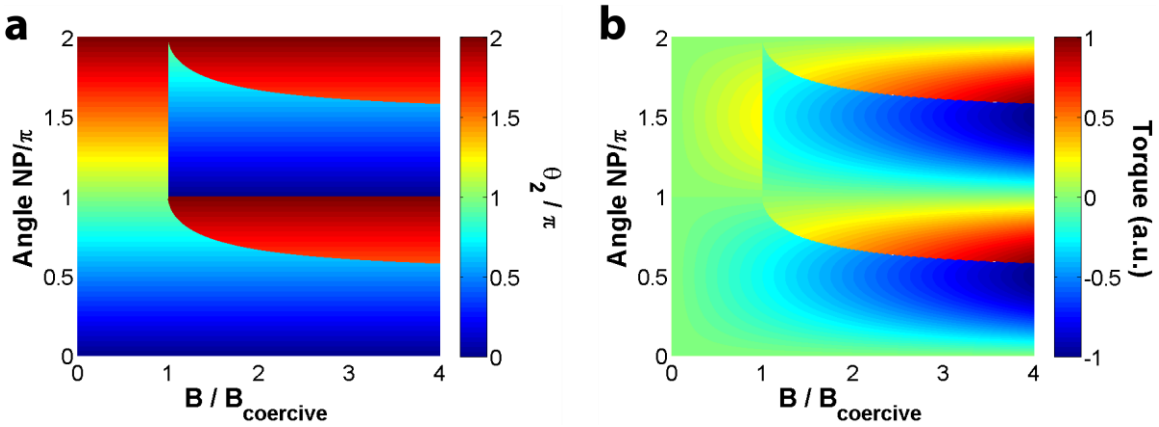

Figure S11 Heat maps for θ_2 and the torque on a nanoparticle with a rectangular hysteresis curve. a) The angle θ_2 between the magnetic moment $\vec{m}$ and the external magnetic field $\vec{B}$ as a function of the orientation of the nanoparticle θ_{NP} and the magnetic field $|\vec{B}|$, or equivalently B/B_{coercive}. b) The torque as a function of the orientation of the nanoparticle θ_{NP} and the magnetic field $|\vec{B}|$, or equivalently B/B_{coercive}.

In the plots, we observe two regimes $B/B_{\text{coercive}} < 1$ and $B/B_{\text{coercive}} > 1$. In the first regime $B < B_{\text{coercive}}$, the magnetic dipole cannot flip between the two aligned states and hence it acts as a permanent dipole. The angle $\theta_2 = \theta_{NP}$ and the torque is 2π-periodic. In the second regime $B > B_{\text{coercive}}$, the magnetic dipole flips, when the component along the anisotropy axis is larger than B_{coercive}. For B/B_{coercive} slightly larger than one, the magnetic dipole only flips near π, while for $B/B_{\text{coercive}} \gg 1$, the dipole flips already just beyond $\pi/2$. The torque is π-periodic.

S4.2 The torsional stiffness as a function of *B*

In Figure S12, we focus on the torque and the torsional stiffness of a nanoparticle with rectangular hysteresis curve. From the plot of the torque in Figure S11.b, we extract the torque as function of θ_{NP} for different values of B/B_{coercive} (Figure S12.a). The derivatives of these curves near $\theta_{NP} = 0$, give the torsional stiffness for different values of B/B_{coercive}, as plotted in Figure S12.b. Near $\theta_{NP} = 0$, the dipole will not flip, so it will act as a permanent moment. The torsional stiffness is therefore expected to be linear in the field $|\vec{B}|$, or equivalently linear in B/B_{coercive}.

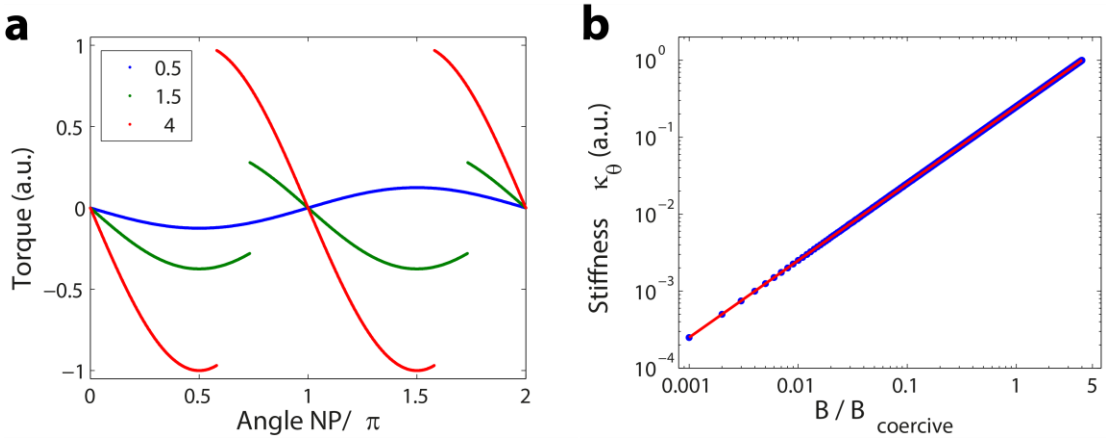

Figure S12 The torsional stiffness at different values of the magnetic field B. a) The torque dependence on θ_{NP} for different values of B/B_{coercive} indicated by the different colours (see legend). b) The torsional stiffness dependence on B/B_{coercive}. The blue dots are the data obtained via Figure S12.a and the red line is a co-plot with slope one.

S4.3 Mapping single nanoparticle behaviour to bead behaviour

When this model was proposed for superparamagnetic beads [9], the authors explicitly included a specific orientation distribution of the nanoparticles inside the bead. Deduction of the bead behaviour from the single nanoparticle behaviour is therefore less trivial than in **S1**-**S3**. Therefore we have simulated the bead behaviour for the current model (bacterial flagellar motor experiment in **S4.3.3** and DNA experiment in **S4.3.4**), starting from our calculations of single nanoparticles (**S4.3.1**), using a forward Euler method (**S4.3.2**).

S4.3.1 The magnetic torque $\tau_{magnets}$ on multiple nanoparticles

In the current model (nanoparticles with the rectangular hysteresis curves), the magnetic torque is given by [9]:

$$\tau_{magnets} = B \sum_{i=1}^{N} \mu_i \sin(\theta_i - \theta_{field}) \qquad \text{S27}$$

where B is the magnetic field, N is the number of nanoparticles, μ_i is the magnitude of the magnetic moment of the ith nanoparticle, θ_i is the orientation of the magnetic moment of the ith nanoparticle, and θ_{field} is orientation of the field. The magnetic moments are assumed to have equal magnitude and to be equally spaced over an angular range less than 180°. In this model, the orientation of the magnetic moment of each nanoparticle θ_i can flip by 180°, if the coercive field is overcome. So at each time step of the simulation, we check for each nanoparticle whether the component of the magnetic field along the anisotropy axis is parallel or antiparallel to the magnetic moment of the nanoparticle, and, if it is antiparallel, whether it is larger than the coercive field. If the component is larger than the coercive field, the magnetic moment flips and we add 180° to θ_i. This is further explained in Figure S13.

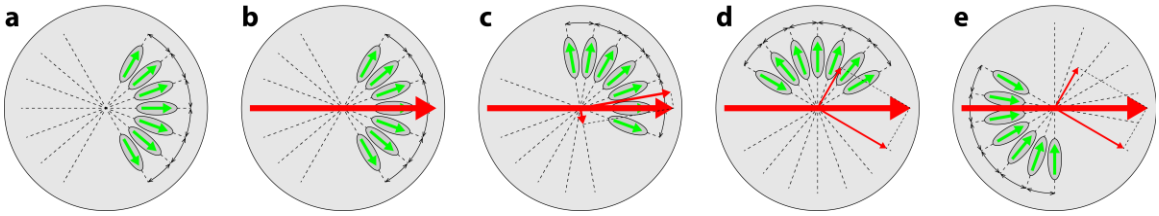

Figure S13 Example of the model with coercive field induced flipping with $N = 7$, $\Delta\theta = 20°$ and $\theta_{field} = 0°$. a) The external magnetic field (red) is off and the magnetic moments (green) of the nanoparticles do not flip thermally. Going from b to e, the particle is rotated in the counter clockwise direction. b) The net magnetic moment is aligned with the magnetic field. c) The bead is rotated and the external magnetic field is now opposing the magnetic moment of one of the nanoparticles. However, the component of the magnetic field along the anisotropy axis of this nanoparticle, is less than the coercive field, so the magnetic moment does not flip. d) Further rotation of the bead with respect to the external field increases the magnetic field component opposing the magnetic moment of the nanoparticle. At this point the opposing field is larger than the coercive field, so the moment flips over 180°. e) Further rotation of the bead will cause the other magnetic moment to flip as well.

For the simulations we use 22 nanoparticles, each with magnetic moment $\mu = 1.1 \cdot 10^{-17}\ Am^2$, and equally spread over 126°, so $\Delta\theta = 6°$ [9].

S4.3.2 Explanation of the numerical approach of simulation

The equation of motion for a superparamagnetic bead in our experiments is given by:

$$\tau_{inertia} = \tau_{drag} + \tau_{external} + \tau_{thermal} \qquad \text{S28}$$

where the different terms describe the torques due to inertia, due to hydrodynamic drag, due to external factors, such as an external magnetic field, and due to thermal fluctuations, respectively.

The torque due to Brownian fluctuations, $\tau_{thermal}$, is given by:

$$\tau_{thermal} = r_n\sqrt{2k_BT\gamma/\Delta t} \quad \text{S29}$$

where r_n is a random number drawn from a Gaussian distribution with $\mu = 0$ and $\sigma = 1$, k_B is the Boltzmann constant, T is the temperature, and Δt is the time step of the simulation.

The value of $\tau_{external}$ depends on the experiment we are trying to simulate. For the bacterial flagellar motor experiments, the external torque is given by $\tau_{external} = \tau_{magnets} + \tau_{motor}$, where $\tau_{magnets}$ is the torque on the bead due to the magnetic field of the magnets (**Equation S27**), and τ_{motor} is the torque on the bead due to the bacterial flagellar motor. For the DNA experiments, the external torque is given by $\tau_{external} = \tau_{magnets} + \tau_{DNA}$, where τ_{DNA} is the torque on the bead that results from the intrinsic torsional stiffness of the DNA molecule. Since the torsional stiffness of the DNA molecule [10,11] is orders of magnitude smaller than the torsional stiffness of the magnetic trap, we may also neglect τ_{DNA}.

Neglecting the inertial torque and using $\tau_{drag} = -\gamma\, d\theta/dt$, the equation of motion can now be rewritten:

$$\gamma\frac{d\theta}{dt} = \tau_{external} + \tau_{thermal} \quad \text{S30}$$

$$\gamma\frac{\theta(t+\Delta t) - \theta(t)}{\Delta t} = \tau_{external} + \tau_{thermal} \quad \text{S31}$$

$$\theta(t+\Delta t) = \theta(t) + \left(\frac{\tau_{external} + \tau_{thermal}}{\gamma}\right)\Delta t \quad \text{S32}$$

We use this equation to perform the simulations.

S4.3.3 Bacterial flagellar motor experiment

In the bacterial flagellar motor experiments, the motor actively rotates the bead inside the magnetic field and essentially provides a full scan of the magnetic potential. The periodicity of the potential will give a very clear distinction among the models or regimes of the models. The details of the angular distributions could then even allow us to distinguish between models/regimes of models with the same periodicity.

Most terms in **Equation S32** have been discussed, i.e. $\tau_{external}$ and $\tau_{thermal}$, but not the drag coefficient γ. For the bacterial flagellar motor experiments, we will assume the bead is spun around by the motor on a circle. The drag coefficient is then expressed as:

$$\gamma = \gamma_{rotational} + \gamma_{translational} \cdot R_{circle}^2 \quad \text{S33}$$

$$\gamma = 8\pi\eta R_{bead}^3 + 6\pi\eta R_{bead}R_{circle}^2 \quad \text{S34}$$

Here we neglect hydrodynamic surface effects. For the bacterial flagellar motor experiments, we used $\eta = 10^{-3}\ Pa \cdot s$, $R_{bead} = 1.05\ \mu m/2$ and $R_{circle} = 250\ nm$, resulting in a value for the drag coefficient $\gamma \approx 4.3\ pN \cdot nm \cdot s$.

The graph shows a π-periodicity.

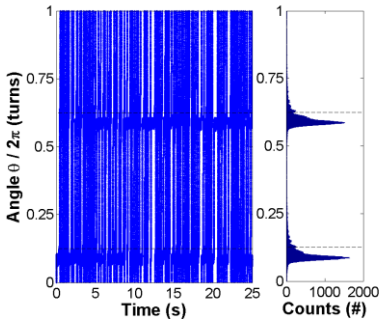

Figure S14 Angular trace and histogram predicted by the model. In the simulations $\Delta t = 25\ \mu s$, total time is 25 s, $\tau_{motor} = 1000\ pN \cdot nm$ and $B = 10\ mT$. The dashed lines represent 45° and 225°. Simulation in which $\tau_{magnets}$ is calculated from Equation S27 with coercive field $B_{\text{coercive}} = 2\ mT$, $N_{NP} = 22$ and the nanoparticles are evenly spread from -63° to 63° in steps of $\Delta\theta = 6°$. The magnetic moments of the nanoparticles was set to $\mu = 1.1 \cdot 10^{-17}\ Am^2$ per nanoparticle to obtain an average rotation speed of the motor of about +5 Hz.

S4.3.4 Angular thermal fluctuations experiment $\tau_{external} = \tau_{magnets}$

In the DNA experiments, the drag coefficient differs from that in the flagellar motor experiments. To compute its value, we first assume that the magnetic bead rotates on axis. Second, the magnetic bead has a fiducial marker bead attached to it, which we assume to rotate on a circle with $R_{circle} = R_{magnetic\ bead} + R_{fiducial\ marker}$. The drag coefficient is then expressed as:

$$\gamma = \gamma_{rotational}^{magnetic\ bead} + \gamma_{rotational}^{fiducial\ marker} + \gamma_{translational}^{fiducial\ marker} \qquad \textbf{S35}$$

$$\gamma = 8\pi\eta R_{magnetic\ bead}^3 + 8\pi\eta R_{fiducial\ marker}^3 + 6\pi\eta R_{fiducial\ marker} R_{circle}^2 \qquad \textbf{S36}$$

Here we neglect hydrodynamic effects due to the proximity of the surface. For the DNA experiments with MyOne beads, we use the dynamic viscosity $\eta = 10^{-3}\ Pa \cdot s$, $R_{magnetic\ bead} = 1.05\ \mu m/2$, and $R_{fiducial\ marker} = 450\ nm/2$. We determine a value for the drag coefficient $\gamma \approx 6.3\ pN \cdot nm \cdot s$.

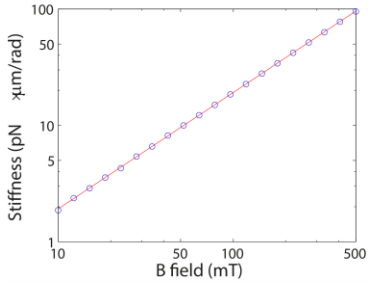

Figure S15 Torsional stiffness κ_θ versus magnetic field B on a log-log scale. In the simulations $\Delta t = 1\ \mu s$ and the total simulated time was 50 s for each value of the field. Model with coercive field induced flipping. The parameters used are the coercive field $B_{\text{coercive}} = 2\ mT$, $N_{NP} = 22$, and the nanoparticles are evenly spread from -63° to 63° in steps of $\Delta\theta = 6°$. The magnetic moments of the nanoparticles is set to $\mu = 1.1 \cdot 10^{-17}\ Am^2$. The red line is $\kappa_\theta = m_{net} B$ where m_{net} is the net magnetic moment of all nanoparticles provided that they do not flip.

The result of the simulations is shown in Figure S15**.** When the angular fluctuations of the bead are sufficiently small, such that the component of the external field along the anisotropy axes of the nanoparticles remains in the same direction as the dipole moments of the nanoparticles, the dipole moments will not flip. Therefore the bead will act as though it has a permanent moment. The red line in Figure S15 represents $\kappa_\theta = m_{net}B$, where

$$m_{net} = \mu \sum_{i=1}^{N} \cos\theta_i \qquad \text{S37}$$

where μ is the magnitude of the magnetic moment of a nanoparticle, i runs from 1 to 22 and θ_i runs from -63° to 63° in steps of $\Delta\theta = 6°$. We find $m_{net} = 1.9 \cdot 10^{-16}\ Am^2$.

S5 Improvements to the proposed theoretical models

We have discussed and quantitatively evaluated several models for the torque on superparamagnetic beads; these models are still idealizations and include a number of simplifications. A more complete model could involve a size distribution of the magnetic nanoparticles. This size distribution will result in a distribution of values of $K = \frac{1}{2}CV$ and $m = MV$, but also in a distribution in Néel relaxation times [7], which will probably give a range of nanoparticle properties going from very paramagnetic to very ferromagnetic on the time scale of the measurement. In addition, there might be a distribution in anisotropy constants independent of the volume, but perhaps more dependent on the source of anisotropy. The orientation distribution of the nanoparticles was already taken into account, but could be made more continuous.
Nonetheless, we find that our current data are well described by the simplified model with superparamagnetic nanoparticles of uniform size. As more data become available, it might become possible to quantitatively test and discriminate between extensions and refinements of our basic models.

S6 Estimation of the magnetic content inside the beads

The composition of MyOne beads has been thoroughly characterized [1]. In particular, the total bead density has been determined to ρ_{bead} = 1.7 g/cm^3, with a Fe mass content of $m_{Fe,total}/m_{bead}$ = 255 mg/g [1]. Moreover, maghemite (Fe_2O_3) has been shown to be the predominant iron oxide phase of the nanoparticles [1]. With a density of maghemite of $\rho_{maghemite}$ = 4.9 g/cm^3, a density of the polystyrene matrix of $\rho_{polystyrene}$ = 1.05 g/cm^3, and a total volume of the bead of $V_{bead} = \frac{4}{3}\pi\left(\frac{1.05}{2}\right)^3\ \mu m^3$ [1], we can estimate the volume fraction of maghemite nanoparticles in the bead, $V_{maghemite}/V_{bead}$, by setting $\rho_{bead}V_{bead} = \rho_{maghemite}V_{maghemite} + \rho_{polystyrene}V_{polystyrene}$ (notice that $V_{polystyrene} = V_{bead} - V_{maghemite}$), yielding a volume fraction of $V_{maghemite}/V_{bead}$ = 17%.

Another way of estimating the volume fraction of magnetic nanoparticles inside the beads is by calculating the mass ratio of maghemite in the beads, $m_{maghemite}/m_{bead}$, as well as their density ratio $\rho_{maghemite}/\rho_{bead}$. The first is simply given by $m_{maghemite}/m_{bead} = m_{Fe,total}/m_{bead}\ (2m_{Fe} + 3m_O)/(2m_{Fe})$, where m_{Fe} is the mass of an iron atom and m_O is the

mass of an oxygen atom. With $V = \rho/m$ we arrive at a volume fraction of $V_{\text{maghemite}}/V_{\text{bead}} = 13\%$.

Assuming spherical nanoparticles of 8 nm in diameter [1], these volume fractions correspond to having $3 \cdot 10^5 - 4 \cdot 10^5$ nanoparticles per MyOne bead.

S7 Torque due to magnetic dipole-dipole interactions

We have found that the magnetic anisotropy of superparamagnetic nanoparticles and a net alignment of their anisotropy axes within the bead can explain the torsional stiffness, which we observe for the superparamagnetic beads in a magnetic field (see the fits to the experimental data in Figure 3f and 3g of the main text). In addition to the magnetic anisotropy of superparamagnetic nanoparticles (NPs), the dipole-dipole interactions between their magnetic moments are a possible origin for the torsional stiffness superparamagnetic beads experience in a magnetic field. NPs in the beads have been found to be partly present in clusters, with a cluster size typically in the 20 nm range [1]. Furthermore, Mössbauer spectra indicate that magnetic properties of iron oxide nanoparticles in Dynabeads are strongly influenced by interparticle interactions [1]. Here we determine whether dipole-dipole interactions between the magnetic moments of superparamagnetic nanoparticles can explain both magnitude and shape of the experimentally observed torsional stiffness. To this end, we assume the NPs to be present in clusters of two NPs, with a net alignment of the particle clusters.

To derive an expression for the torque due to magnetic dipole-dipole interactions between NPs and a net orientation of NP clusters, we first have to find an expression for the free energy of one NP cluster. The relevant terms are the dipole-dipole interaction energy of a NP cluster composed of N_k NPs and the magnetic energy to align the magnetic moment $\vec{m}$ with the magnetic field $\vec{B}$:

$$U_{N_k} = \frac{\mu_0 \mu_S}{4\pi} \frac{(MV)^2}{r_k^3} (1 - 3\cos^2\theta_1) - N_k BMV\cos(\theta - \theta_1), \qquad \text{S38}$$

where r_k is the particle distance in the cluster given by $\frac{1}{r_k^3} = \sum_{i=1}^{N_{k-1}} \sum_{j=i+1}^{N_k} \frac{1}{r_{ij}^3}$ (r_{ij} is the distance between particle i and j), V the NP volume, M the NP magnetization, and B the magnetic field strength. θ_1 is the angle between the magnetic moment and the anisotropy axis and θ the angle between the magnetic field and the anisotropy axis, as shown in Figure S16.a.

If we assume that all N_{Cl} NP clusters in the bead are aligned with their anisotropy axes pointing in the same direction (we therefore consider effective values for the magnetization), the total energy of the magnetic bead writes

$$U_{\text{tot}} = N_{\text{Cl}} U_{N_k}. \qquad \text{S39}$$

The equilibrium orientation of the magnetic moment $\vec{m}$, $\theta_1(N_k, r_k, V, M, B, \theta)$, is determined by setting $\frac{\partial U\text{tot}}{\partial \theta_1} = 0$ (θ_1 is assumed to be small). We then arrive at an expression for the torque $\Gamma_{mag} = -\frac{\partial U\text{tot}}{\partial \theta}$ which, assuming small θ, can be written similar to **Equation 3** (main text), namely

$$\Gamma_{\mathrm{mag}} = -N_{\mathrm{Cl}} N_{\mathrm{k}} V \frac{C'(M) B M}{(C'(M) + B M)} \theta = -\kappa_{\theta}\, \theta, \qquad \text{S40}$$

with $C'(M(B)) = \frac{\mu_0 \mu_S}{4\pi} \frac{6}{N_k} \frac{M(B)^2 V}{r_k^3}$.

In contrast to the model considering magnetic NP anisotropy (**Equation 3** of the main text), now C is not a material constant, but rather a function of the cluster size (i.e. the number of NPs composing the cluster), the distance between particles in the cluster, and the magnetization.

To achieve a good fit of this model to the experimental data, the shape of the magnetization curve turned out to be critical. Not necessarily all NPs in the bead contribute to the magnetic anisotropy, so the total magnetization $M(B)$ consists of an isotropic and an anisotropic part, of which here only the anisotropic part is relevant. In particular, anisotropy leads to a smoother increase of the $M(B)$ curve [12]. We therefore assumed $M(B)$ to be of Langevin shape $\left(M(B) = M_{sat}(\coth(B/B_0) - B_0/B)\right)$, where B_0 was a global fit parameter (and thus equal for all beads of the same bead type). The number of NP clusters in one bead, N_{Cl}, on the other hand, was a free fit parameter for each bead. The remaining parameters of **Equation S40** were set to the following values: clusters were assumed to consist of two NPs ($N_k = 2$) and the distance between particles in the cluster was set to twice the average NP radius (i.e. 8 nm, meaning that the two NPs are stuck to each other). The volume V of a NP was assumed to be that of a sphere of 8 nm in diameter, and M_{sat} was set to the values obtained by measurements of dried powder with a Vibrating Sample Magnetometer (namely $M_{sat} = 43\ kA/m$ (MyOne) and $M_{sat} = 28\ kA/m$ (M270)) [6].

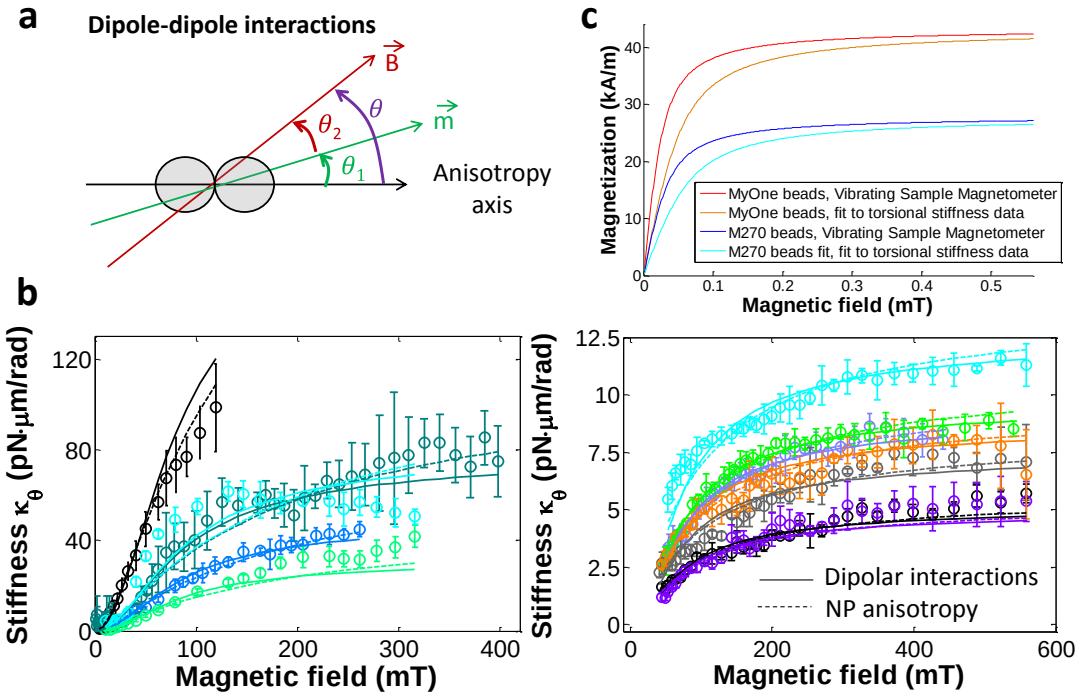

Figure S16 a) Schematic illustrating magnetic dipole-dipole interactions in a nanoparticle cluster. b) Torsional stiffness measured (open circles) for two types of superparamagnetic beads (M270 beads, left panel, and MyOne beads, right panel), fitted by

the model considering dipole-dipole interactions between the magnetic moments of superparamagnetic nanoparticles (solid line). For comparison, the fit with the model taking into account the magnetic anisotropy of superparamagnetic nanoparticles is also shown (dashed line). c) Comparison of the magnetization curves obtained by measurements of dried bead powder with a Vibrating Sample Magnetometer, which contains both isotropic and anisotropic contributions, and the magnetization curve yielding the best fit of the dipole-dipole interaction model to the torsional stiffness data, which represents the anisotropic part of the magnetization.

The dipolar interaction model yields a good fit to the torsional stiffness data we obtained for two different types of superparamagnetic beads (namely M270 beads and MyOne beads, both from Dynabeads®) (Figure S16.b, same experimental data as shown in **Figure 3f** and **Figure 3g** of the main text). The fits yield $B_0 = 23$ mT (MyOne beads, $\chi^2_{\mathrm{red}} = 1.8$) and $B_0 = 28\,mT$ (M270 beads, χ^2_{red} = 3.2), which corresponds to a more gradual increase of the magnetization with the magnetic field compared with the magnetization curve obtained by measurements of dried bead powder with a Vibrating Sample Magnetometer (B_0 = 12 mT (MyOne) and B_0 = 16 mT (M270)) [6] (Figure S16.c). The total number of NP dimers, N_{cl}, were determined from the fits to 3 to $8{\cdot}10^4$ (MyOne), which is less than half of the total estimated number of NPs included in these beads (see section S7), and 0.5 to $3.2{\cdot}10^6$ (M270). Consequently, dipolar interactions of superparamagnetic NPs in the beads can account for the order of magnitude of the experimentally observed torque.

In conclusion, both the magnetic anisotropy of superparamagnetic nanoparticles and the dipole-dipole interactions between their magnetic moments can explain the torsional stiffness observed for superparamagnetic beads in a magnetic field. In fact, both may yield significant contributions to the torsional stiffness. As for a prediction of torque and its dependence on the magnetic field, either model can serve to estimate the curve shape for any bead type of similar characteristics (i.e. containing NPs with similar magnetic properties and a similar distribution in a non-magnetic matrix).

S8 Experimentally determined stable trapping positions

In the main text, we used a magnetic bead attached to a bacterial flagellar motor to scan the magnetic potential. Here, we employ an alternative approach to determine the periodicity of the magnetic potential. In this approach, we do not scan the full potential, but instead we locate the minima in the potential, as stable trapping positions.

In this experiment, we start with the magnets far from the sample plane, so that the flagellar motor can freely rotate the magnetic bead. Then we increase the external field strength rapidly by moving the magnets close to the sample plane, such that the motor stalls. Subsequently, we move the magnets away from the sample plane and repeat the cycle. Several such “rotate and stall” cycles were carried out for different magnet orientations (Figure S17).

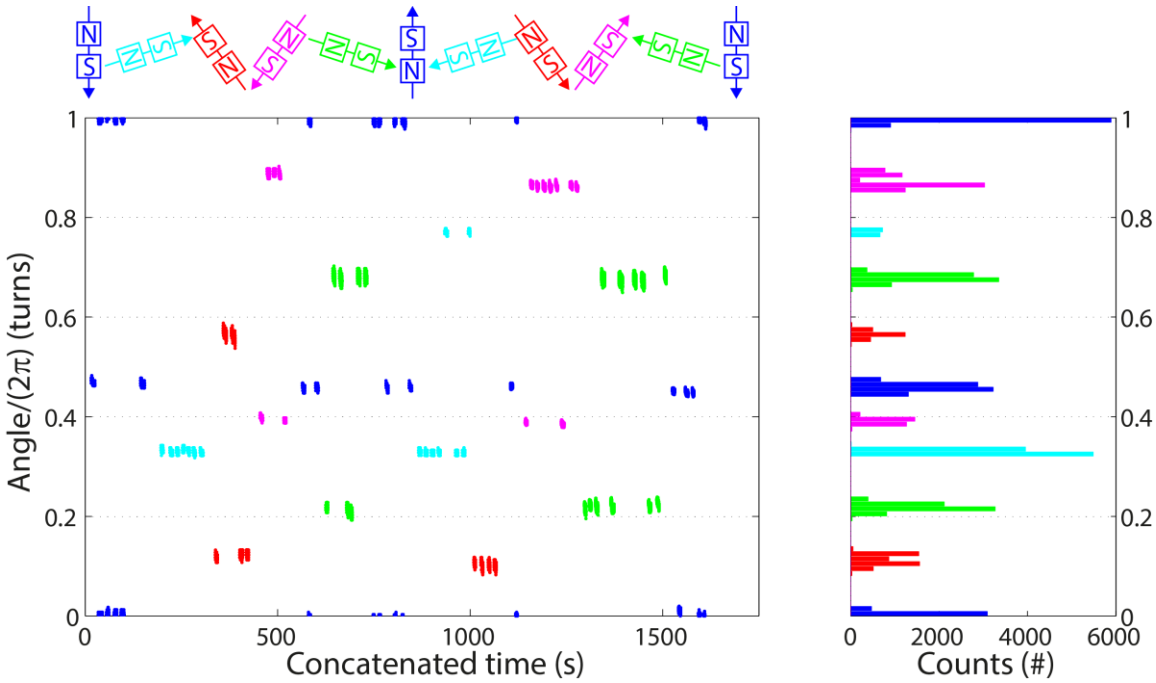

Figure S17 Stall positions of the bacterial flagellar motor at different magnet orientations. a) Angle as a function of time. Only the bead positions with the magnets close to the sample plane are shown, so each cluster of data points is a stall event in the "rotate and stall" cycle. The bead positions during magnet movement and magnet far away from the sample plane are omitted. The different colours indicate different magnet orientations. b) Histogram of the data in (a).

As the magnets approach the sample plane, the magnetic bead becomes trapped in a local potential well of the magnetic potential. The fact that we consistently observe two stable trapping positions, which are separated by 0.50±0.05 turns, suggests again that the magnetic potential is π-periodic. When we bring the magnets very close to the sample plane, higher fields than in the assay described in the main text are imposed, which explains the small angular fluctuations at the stall positions of the motor.

S9 Measurement of the standard deviation versus magnet distance

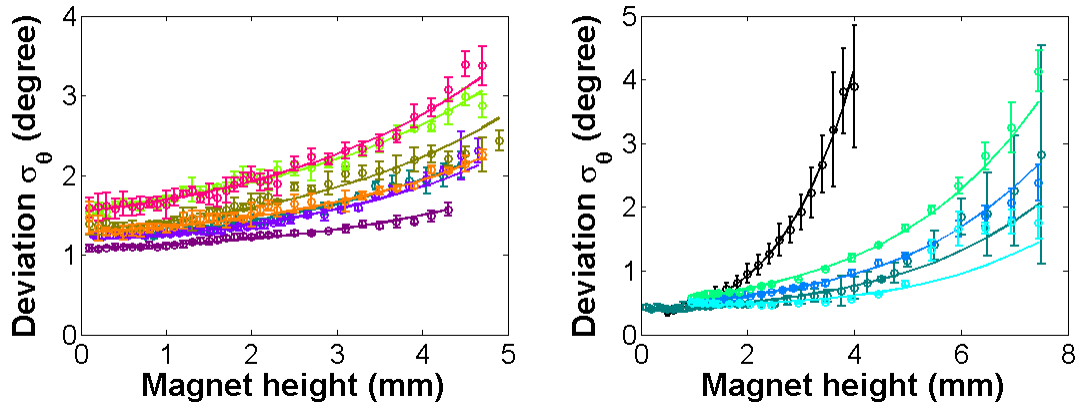

Figure S18 The standard deviation in the angular thermal fluctuations as a function of magnet height above the sample plane. a) MyOne. Colour coding is the same as in the main text. b) M270. Colour coding is the same as in the main text.

From these two plots, we converted the magnet height to magnetic field using a calibrated conversion table and the standard deviation to stiffness by means of the equipartition theorem to obtain Figure 3f and Figure 3g of the main text.

S10 Magnetization

For the model with the superparamagnetic nanoparticles, the magnetization $|\vec{M}|$ in **Equation 3** of the main text is dependent on the magnetic field $|\vec{B}|$. We approximate the magnetization $|\vec{M}|$ by a Langevin function (**Equation S23**) as fitted to vendor supplied data. For the volume magnetization of MyOne beads, we use $M_{sat} = 43.3\ kA/m$ and $B_0 = 12\ mT$ [6]. For the magnetization of M270 beads, we use $M_{sat} = 27.9\ kA/m$ and $B_0 = 15.5\ mT$ [13].

S11 Minimizing the effects of the camera integration time

The thermal angular fluctuations of the magnetic bead are used to calculate the torsional stiffness experienced by the bead in the magnetic field by means of the equipartition theorem: $\kappa_\theta = k_B T/\langle\theta^2\rangle$. Due to a finite integration time/exposure time of the camera, the angular fluctuations are averaged. The angular fluctuations $\langle\theta^2\rangle$ will then be underestimated, and hence the torsional stiffness κ_θ will be overestimated. Reducing the exposure time reduces this averaging effect or blurring.

Motion blurring occurs because of motion during the acquisition of a single image. As the bead moves, its motion is averaged over one exposure time, hence the image is blurred [14]. The degree of blurring depends on the ratio between the exposure time τ_{expo} and the characteristic time τ_c of the bead, $\alpha = \tau_{expo}/\tau_c$, where the characteristic time is defined as $\tau_c = \gamma_\theta/\kappa_\theta$ with the rotational drag coefficient of the bead γ_θ (**Equation S36**) and the torsional trap stiffness κ_θ. The effect of blurring is that the measured fluctuations $\langle\theta^2\rangle_{meas}$ are different from the actual fluctuations $\langle\theta^2\rangle$. The measured fluctuations are given by [15]. The measured variance approximates the actual variance best, if the exposure time τ_{expo} is much shorter than the characteristic time τ_c.

For our measurements of the torsional stiffness, we can estimate the rotational drag coefficients for MyOne and M270 beads based on **Equation S36** and then estimate the characteristic time using the measured torsional stiffness. The rotational drag coefficient for MyOne beads we estimate to be $\gamma \approx 6.3\ pN \cdot nm \cdot s$ and for M270 beads $\gamma \approx 106\ pN \cdot nm \cdot s$. These values are probably lower limits, since the drag will increase, if the beads do not rotate exactly on-axis. The saturation stiffness for MyOne is $\kappa_{\theta,\max} = 9.5\ pN \cdot \mu m/rad$ and for M270 $\kappa_{\theta,\max} = 133\ pN \cdot \mu m/rad$ (see main text). The characteristic times are then $\tau_c \approx 660\ \mu s$ and $\tau_c \approx 800\ \mu s$ for MyOne and M270, respectively. In order to have a <10% deviation from the actual value, the exposure time τ_{expo} needs to be at least three times smaller than the characteristic time τ_c. In our experiments, we use an exposure time of $\tau_{expo} = 200\ \mu s$ in order to approximate the actual variance reasonably well. We note that the sampling interval can be much larger

than the exposure time and that the total measurement time should be sufficiently large for the bead to explore the full magnetic potential.

Supplementary References

[1] G. Fonnum, C. Johansson, A. Molteberg, S. Mørup, and E. Aksnes, J. Magn. Magn. Mater. **293**, 41 (2005).

[2] G. Mihajlović, K. Aledealat, P. Xiong, S. von Molnár, M. Field, and G. J. Sullivan, Appl. Phys. Lett. **91**, 172518 (2007).

[3] E. C. Stoner and E. P. Wohlfarth, Philos. Trans. R. Soc. A Math. Phys. Eng. Sci. **240**, 599 (1948).

[4] D. Normanno, M. Capitanio, and F. S. Pavone, Phys. Rev. A **70**, 053829 (2004).

[5] V. I. Lebedev and D. N. Laikov, Dokl. Math. **59**, 477 (1999).

[6] J. Lipfert, X. Hao, and N. H. Dekker, Biophys. J. **96**, 5040 (2009).

[7] A. H. Morrish, *The Physical Principles of Magnetism* (IEEE, 2001).

[8] X. J. A. Janssen, A. J. Schellekens, K. van Ommering, L. J. van IJzendoorn, and M. W. J. Prins, Biosens. Bioelectron. **24**, 1937 (2009).

[9] A. van Reenen, F. Gutiérrez-Mejía, L. J. van IJzendoorn, and M. W. J. Prins, Biophys. J. **104**, 1073 (2013).

[10] J. Lipfert, J. W. J. Kerssemakers, T. Jager, and N. H. Dekker, Nat. Methods **7**, 977 (2010).

[11] Z. Bryant, M. D. Stone, J. Gore, S. B. Smith, N. R. Cozzarelli, and C. Bustamante, Nature **424**, 338 (2003).

[12] M. Hanson, C. Johansson, and S. Mørup, J. Phys. Condens. Matter **5**, 725 (1993).

[13] J. Lipfert, M. Wiggin, J. W. J. Kerssemakers, F. Pedaci, and N. H. Dekker, Nat. Commun. **2**, 439 (2011).

[14] A. J. W. te Velthuis, J. W. J. Kerssemakers, J. Lipfert, and N. H. Dekker, Biophys. J. **99**, 1292 (2010).

[15] W. P. Wong and K. Halvorsen, Opt. Express **14**, 12517 (2006).